

Cross-modality image synthesis from unpaired data using CycleGAN

Effects of gradient consistency loss and training data size

Yuta Hiasa¹, Yoshito Otake¹, Masaki Takao², Takumi Matsuoka¹, Kazuma Takashima², Jerry L. Prince³ Nobuhiko Sugano², and Yoshinobu Sato¹

¹ Graduate School of Information Science, Nara Institute of Science and Technology
8916-5, Takayamacho, Ikomashi, Nara 630-0192, Japan
hiasa.yuta.ht7@is.naist.jp

² Graduate School of Medicine, Osaka University

³ Department of Electrical and Computer Engineering, Johns Hopkins University

Abstract. CT is commonly used in orthopedic procedures. MRI is used along with CT to identify muscle structures and diagnose osteonecrosis due to its superior soft tissue contrast. However, MRI has poor contrast for bone structures. Clearly, it would be helpful if a corresponding CT were available, as bone boundaries are more clearly seen and CT has standardized (i.e., Hounsfield) units. Therefore, we aim at MR-to-CT synthesis. The CycleGAN was successfully applied to unpaired CT and MR images of the head, these images do not have as much variation of intensity pairs as do images in the pelvic region due to the presence of joints and muscles. In this paper, we extended the CycleGAN approach by adding the gradient consistency loss to improve the accuracy at the boundaries. We conducted two experiments. To evaluate image synthesis, we investigated dependency of image synthesis accuracy on 1) the number of training data and 2) the gradient consistency loss. To demonstrate the applicability of our method, we also investigated a segmentation accuracy on synthesized images.

Keywords: Image synthesis, CycleGAN, Musculoskeletal image, MR, CT, Segmentation

1 Introduction

Computed tomography (CT) is commonly used in orthopedic procedures [1]. Magnetic resonance imaging (MRI) is used along with CT to identify muscle structures and diagnose osteonecrosis due to its superior soft tissue contrast [2]. However, MRI has poor contrast for bone structures. Clearly, it would be helpful if a corresponding CT were available, as bone boundaries are more clearly seen and CT has standardized (i.e., Hounsfield) units. Considering radiation exposure in CT, it is preferable if we can delineate boundaries of both muscle and bones in MRI. Therefore, we aim at MR-to-CT synthesis.

Image synthesis has been extensively studied using the patch-based learning [3] as well as deep learning, specifically, convolutional neural networks (CNN) [4] and generative adversarial networks (GAN) [5]. The conventional approaches required the paired training data, i.e., images from multiple modalities that are registered, which limited the application. A method recently proposed by Zhu et al. [6] utilizes unpaired training data by appreciating the cycle consistency loss function, which is called CycleGAN. CycleGAN has already applied to MR-to-CT synthesis [7]. All those previous approaches in medical image application targeted CT and MRI of the head in which the scan protocol (i.e., field-of-view (FOV) and the head orientation within the FOV) is relatively consistent resulting in a small variation in the two image distributions even without registration, thus a small number of training data set (20 to 30) allowed a reasonable accuracy. On the other hand, our target anatomy, the hip region, has larger variation in the anatomy as well as their pose (i.e., joint angle change and deformation of muscles).

Another significant aspect of application of image synthesis is segmentation. Previous studies addressed this problem [8,9], but there were problems which MRI is often taken by multiple sequences and devices, and there is no standard unit as in CT. Therefore, label data are necessary for training of the segmentation method for each sequence and each imaging device. Thus, perfectly MR-to-CT synthesis realizes modality independent segmentation [10].

In this study, we extend the CycleGAN approach by adding the gradient consistency loss and using an order-of-magnitude larger training data set (302 MR and 613 CT volumes) in order to overcome the larger variation and improve the accuracy at the boundaries. We investigated dependency of image synthesis accuracy on 1) the number of training data and 2) the GC loss. To demonstrate the applicability of our method, we also investigated a segmentation accuracy on synthesized images.

2 Method

2.1 Materials

The datasets we used in this study are MRI dataset consists of 302 unlabeled volumes and CT dataset consists of 613 unlabeled, and 20 labeled volumes which are associated with manual segmentation labels of 19 muscles, pelvis, femur and sacrum structures. Patients with implant artifacts in volumes were excluded. As an evaluation dataset, we also used other 10 MR volumes associated with manual segmentation labels of gluteus medius, and minimus muscles, pelvis and femur structures, as the ground truth. MR volumes were scanned for diagnosis of osteonecrosis by a 1.0T MR imaging system. The T1-weighted volumes were obtained by 3D spoiled gradient recalled echo sequence (SPGR) with a repetition time (TR) of 7.9 ms, echo time (TE) of 3.08 ms, and flip angle of 30. The field of view was 320 mm, and the matrix size was 256×256. The slab thickness was 76 mm, and the slice thickness was 2 mm without an inter-slice gap. CT volumes were scanned for total hip arthroplasty (THA) surgery. The field of view was

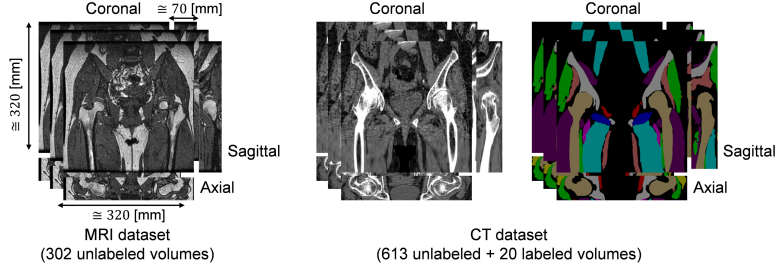


Fig. 1. Training datasets used in this study. MRI dataset consists of 302 unlabeled volumes and CT dataset consists of 613 unlabeled and 20 labeled volumes. N4ITK intensity inhomogeneity correction [11] was applied to all MRI volumes. Two datasets have similar field-of-view, although these are not registered.

360×360 mm and the matrix size was 512×512. The slice thickness was 2.0 mm for the region including pelvis and proximal femur, 6.0 mm for the femoral shaft region, and 1.0 mm for the distal femur region. In this study, the CT volumes were cropped so that the FOV resembles that of MRI volumes, as shown in Figure 1, and then resized to 256×256.

2.2 Image synthesis using CycleGAN with gradient-consistency loss

The underlying algorithm of the proposed MR-to-CT synthesis follows that of Zhu et al [6] which allows to translate an image from a CT domain to a MR domain without pairwise aligned CT and MR training images of the same patient. The workflow is shown in Figure 2. The networks G_{CT} and G_{MR} are generators to translate real MR and CT images to synthesized CT and MR images, respectively. The networks D_{CT} and D_{MR} are discriminators to distinguish between real and synthesized images. While discriminators try to distinguish synthesized images by maximizing adversarial losses \mathcal{L}_{CT} and \mathcal{L}_{MR} , defined as

$$\mathcal{L}_{CT} = \sum_{x \in I_{CT}} \log D_{CT}(x) + \sum_{y \in I_{MR}} \log(1 - D_{CT}(G_{CT}(y))), \quad (1)$$

$$\mathcal{L}_{MR} = \sum_{y \in I_{MR}} \log D_{MR}(y) + \sum_{x \in I_{CT}} \log(1 - D_{MR}(G_{MR}(x))), \quad (2)$$

generators try to synthesize images which is indistinguishable from target domain by minimizing these losses, where x and y are images from domains I_{CT} and I_{MR} . However, networks with large enough capacity leads to translate the same set of images from source domain to any random permutation of images in the target domain. Thus, adversarial losses alone cannot guarantee that the learned generator can translate an individual input to a desired output. Therefore, the loss function is regularized by cycle consistency. Cycle consistency is difference between real and reconstructed image, which is the inverse mapping of synthesized image [6]. The cycle consistency loss \mathcal{L}_{Cycle} is defined as

$$\mathcal{L}_{Cycle} = \sum_{x \in I_{CT}} |G_{CT}(G_{MR}(x)) - x| + \sum_{y \in I_{MR}} |G_{MR}(G_{CT}(y)) - y| \quad (3)$$

We extended the CycleGAN approach by explicitly adding the gradient consistency loss (GC loss) between real and synthesized image to improve the accuracy at the boundaries. The gradient correlation (GC) [12] has been used as

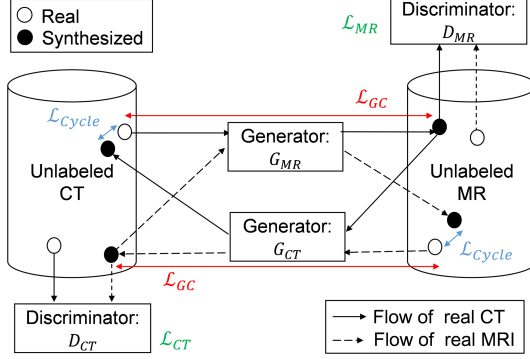


Fig. 2. Workflow of the proposed method. G_{CT} and G_{MR} are generator networks that translates MR to CT images, and CT to MR images, respectively. D_{CT} and D_{MR} are discriminator networks to distinguish between real and synthesized images. The cycle consistency loss \mathcal{L}_{Cycle} is a regularization term which is difference between real and reconstructed image. To improve the accuracy at the boundaries, loss function is regularized by gradient consistency loss \mathcal{L}_{GC} .

a similarity metric in the medical image registration committee. GC is the normalized cross correlation between two images. Given gradients in horizontal and vertical directions of two images, A and B , GC is defined as

$$GC(A, B) = \frac{1}{2} \{ NCC(\nabla_x A, \nabla_x B) + NCC(\nabla_y A, \nabla_y B) \} \quad (4)$$

$$\text{where, } NCC(A, B) = \frac{\sum_{(i,j)} (A - \bar{A})(B - \bar{B})}{\sqrt{\sum_{(i,j)} (A - \bar{A})^2} \sqrt{\sum_{(i,j)} (B - \bar{B})^2}}$$

and ∇_x and ∇_y are the gradient operator of each direction, \bar{A} is the mean value of A . We formulate a gradient-consistency loss \mathcal{L}_{GC} as

$$\mathcal{L}_{GC} = \frac{1}{2} \left\{ \sum_{x \in I_{CT}} (1 - GC(x, G_{MR}(x))) + \sum_{y \in I_{MR}} (1 - GC(y, G_{CT}(y))) \right\} \quad (5)$$

Finally, our objective function is defined as:

$$\mathcal{L}_{total} = \mathcal{L}_{CT} + \mathcal{L}_{MR} + \lambda_{Cycle} \mathcal{L}_{Cycle} + \lambda_{GC} \mathcal{L}_{GC} \quad (6)$$

where λ_{Cycle} and λ_{GC} are weights to balance each loss. Then, we solve:

$$\hat{G}_{MR}, \hat{G}_{CT} = \arg \min_{G_{CT}, G_{MR}} \max_{D_{CT}, D_{MR}} \mathcal{L}_{total} \quad (7)$$

In this paper, we used 2D CNN with 9 residual blocks for generator proposed in [13]. For discriminators, we used 70×70 PatchGAN [14]. We replaced the Eq. (1) and Eq. (2) by least-squares loss as in [15]. These settings follows [6,7]. The CycleGAN was trained using Adam [16] for first 1×10^5 iterations at fixed learning rate of 0.0002, and last 1×10^5 iterations at learning rate which linearly reducing to zero. The balancing weights were empirically determined as $\lambda_{Cycle} = 3$ and $\lambda_{GC} = 0.3$.

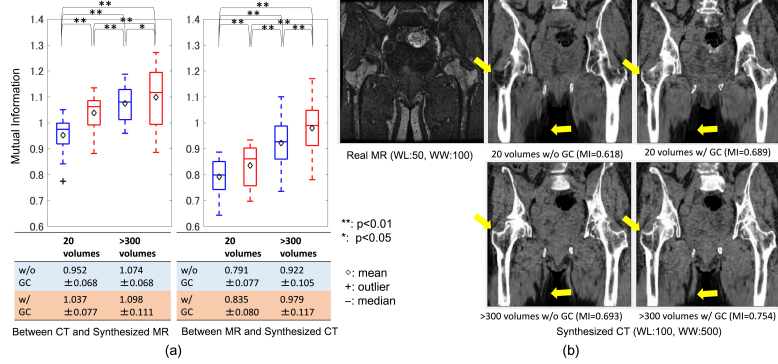


Fig. 3. Evaluation of similarity between the real and synthesized volumes. (a) quantitative comparison on different training data size with and without the gradient-consistency loss by mutual information. (b) representative result of one patient.

3 Result

3.1 Quantitative evaluation on image synthesis

To evaluate image synthesis, we investigated dependency of image synthesis accuracy on the number of training data and the GC loss. The CycleGAN was trained with different sized datasets, i) 20 MR and 20 CT volumes, ii) 302 MR and 613 CT volumes, and both with and without GC loss. Then, model was tested with 10 MR and 20 CT volumes. Since no perfectly registered volumes are available, mutual information (MI) was used as evaluation metric of similarity between the real and synthesized volume.

The quantitative results are shown in Fig.3(a). The left is the box and whisker plots of the mean of each slice of MI between real CT and synthesized MR (i.e., 20 data points in total). The right is the mean of MI between real MR and synthesized CT (i.e., 10 data points in total). The result shows that more training data yielded statistically significant improvement ($p < 0.01$) of paired t -test in MI. The GC loss also leads to an increase in MI between MR and synthesized CT ($p < 0.01$). Fig.3(b) and Fig.4 show examples of the visualization of real MR and synthesized CT volumes. As indicated by arrows, we can see that synthesized volumes with GC loss preserved the shape near the femoral head and adductor muscles.

3.2 Quantitative evaluation on segmentation

To demonstrate the applicability of image synthesis, we also evaluate the segmentation accuracy. Twenty labeled CT datasets were used to train the segmentation network. Then, we evaluated the segmentation accuracy with 10 MR volumes that consist of manual segmentation labels of gluteus medius and minimus muscles and femur.

We employed the 2D U-net architecture proposed by Ronneberger et al. [17] as segmentation network, which is widely used in medical image analysis and

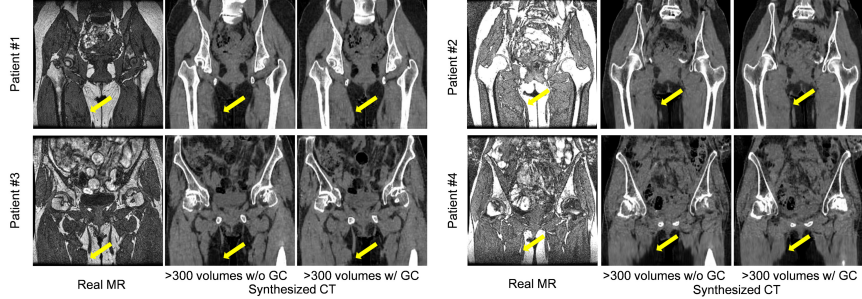


Fig. 4. Representative results of real MR to synthesized CT from four patients with and without the gradient consistency loss. As indicated by arrows, we can see that synthesized volumes with gradient consistency loss preserved the shape near the adductor muscles.

demonstrated high performance with a limited number of labeled volumes. In MRI, muscle boundaries are clearer while bone boundaries are clearer in CT. To incorporate both CT and MR advantage, we modified the 2D U-net to take two-channel input of both CT and synthesized MR images. We trained on 2D U-net using Adam [16] for 1×10^5 iterations at learning rate of 0.0001. At the test phase, a pair of MR and synthesized CT was used as two-channel input.

The results with 4 musculoskeletal structures and 10 patients are shown as box and whisker plot in Fig.5 (i.e., 10 data points in total on each plot). The result shows that more training data yielded statistically significant improvement in DICE on pelvis, femur, glutes medius ($p < 0.01$) and glutes minimus regions ($p < 0.05$) of paired t -test. The GC loss also leads to an increase in DICE on glutes minimus regions ($p < 0.01$). The average DICE coefficient in the cases trained with more than 300 cases and GC loss was 0.808 ± 0.036 (pelvis), 0.883 ± 0.029 (femur), 0.804 ± 0.040 (gluteus medius) and 0.669 ± 0.054 (gluteus minimus), respectively. Fig.6 shows examples of the visualization of real MR and synthesized CT and esimated label for one patient. The result with GC loss has smooth segmentation not only in the gluteus maximus but also near the adductor muscles.

4 Discussion and Conclusion

In this study, we proposed a image synthesis method which extended the CycleGAN approach by adding the GC loss to improve the accuracy at the boundaries. Specifically, the contributions of this paper are 1) introduction GC loss in CycleGAN, and 2) investigation of the dependency of both image synthesis accuracy and segmentation accuracy on the large number of training data. One limitation of this study is quantitative evaluation of the accuracy of image synthesis due to the lack of paired ("registered") volumes of the same patient. Another limitation is that in clinical situation some patients would have implants, which the datasets in this study does not include. As a comparison, we performed 5-fold cross validation of MR segmentation with labeld 10 MR volumes (i.e., trained

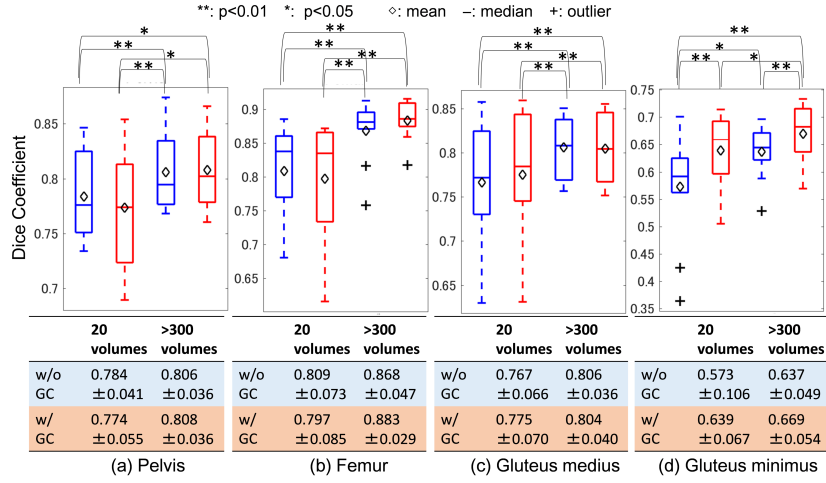


Fig. 5. Evaluation of segmentation accuracy on different training data size in CycleGAN with and without the gradient-consistency loss. Segmentation of (a) pelvis, (b) femur, (c) gluteus medius and (d) gluteus minimus muscle in MR volumes were performed using MR-to-CT synthesis.

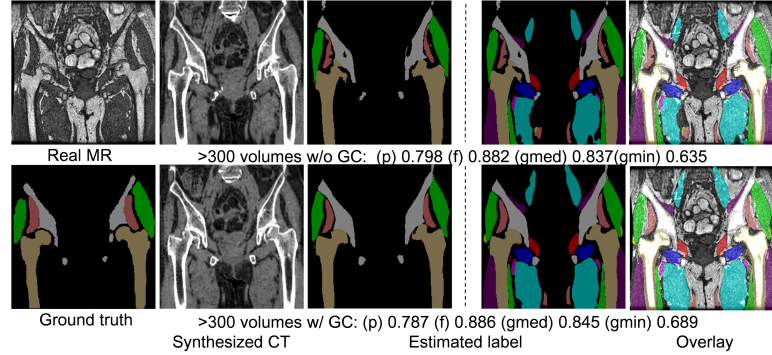


Fig. 6. Representative results of segmentation from one patient. The ground truth label is consist of 4 musculoskeletal structures in MRI. Although we evaluated only on 4 structures because ground truth were not available for the other structures on MRI, all 22 estimated labels are shown for qualitative evaluation. In the right-most column, all estimated labels are overlaid on the real MRI. p, f, gmed, gmin denote DICE of pelvis, femur, gluteus maximus, and gluteus minimus, respectively.

with 8 MR volumes and then tested remaining 2 MR volumes) using U-net segmentation network. The DICE was 0.815 ± 0.046 (pelvis), 0.921 ± 0.023 (femur), 0.825 ± 0.029 (gluteus medius) and 0.752 ± 0.045 (gluteus minimus), respectively. A potential improvement of modality independent segmentation is to construct an end-to-end network that performs image synthesis and segmentation [18]. Our future work also include development of effective incorporate the CT and MR infomation to improve segmentation accuracy.

References

1. Beaulé, P.E., et al.: Three-dimensional computed tomography of the hip in the assessment of femoroacetabular impingement. *Journal of orthopaedic research* **23**(6) (2005) 1286–1292
2. Cvitanic, O., et al.: Mri diagnosis of tears of the hip abductor tendons (gluteus medius and gluteus minimus). *American Journal of Roentgenology* **182**(1) (2004) 137–143
3. Torrado-Carvajal, A., et al.: Fast patch-based pseudo-ct synthesis from t1-weighted mr images for pet/mr attenuation correction in brain studies. *Journal of Nuclear Medicine* **57**(1) (2016) 136–143
4. Zhao, C., et al.: Whole brain segmentation and labeling from ct using synthetic mr images. In: *International Workshop on Machine Learning in Medical Imaging*, Springer (2017) 291–298
5. Kamnitsas, K., et al.: Unsupervised domain adaptation in brain lesion segmentation with adversarial networks. In: *International Conference on Information Processing in Medical Imaging*, Springer (2017) 597–609
6. Zhu, J.Y., et al.: Unpaired image-to-image translation using cycle-consistent adversarial networks. In: *Proceedings of the IEEE Conference on Computer Vision and Pattern Recognition*. (2017) 2223–2232
7. Wolterink, J.M., et al.: Deep mr to ct synthesis using unpaired data. In: *International Workshop on Simulation and Synthesis in Medical Imaging*, Springer (2017) 14–23
8. Gilles, B., et al.: Musculoskeletal mri segmentation using multi-resolution simplex meshes with medial representations. *Medical image analysis* **14**(3) (2010) 291–302
9. Ranzini, M.B.M., et al.: Joint multimodal segmentation of clinical ct and mr from hip arthroplasty patients. In: *International Workshop and Challenge on Computational Methods and Clinical Applications in Musculoskeletal Imaging*, Springer (2017) 72–84
10. Hamarneh, G., et al.: Simulation of ground-truth validation data via physically-and statistically-based warps. In: *International Conference on Medical Image Computing and Computer-Assisted Intervention*, Springer (2008) 459–467
11. Tustison, N.J., et al.: N4itk: improved n3 bias correction. *IEEE transactions on medical imaging* **29**(6) (2010) 1310–1320
12. Penney, G.P., et al.: A comparison of similarity measures for use in 2-d-3-d medical image registration. *IEEE transactions on medical imaging* **17**(4) (1998) 586–595
13. Johnson, J., et al.: Perceptual losses for real-time style transfer and super-resolution. In: *European Conference on Computer Vision*, Springer (2016) 694–711
14. Isola, P., et al.: Image-to-image translation with conditional adversarial networks. *arXiv preprint* (2017)
15. Mao, X., et al.: Multi-class generative adversarial networks with the l2 loss function. *CoRR*, abs/1611.04076 **2** (2016)
16. Kingma, D.P., et al.: Adam: A method for stochastic optimization. *arXiv preprint arXiv:1412.6980* (2014)
17. Ronneberger, O., et al.: U-net: Convolutional networks for biomedical image segmentation. In: *International Conference on Medical image computing and computer-assisted intervention*, Springer (2015) 234–241
18. Huo, Y., et al.: Adversarial synthesis learning enables segmentation without target modality ground truth. *arXiv preprint arXiv:1712.07695* (2017)